ARTICLE

Cavity-Enhanced Saturation Spectroscopy of Molecules with sub-kHz Accuracy†

Tian-peng Hua[a], Yu Robert Sun[a,b], Jin Wang[a,b], Chang-le Hu[a], Lei-gang Tao[a], An-wen Liu[a,b], Shui-ming Hu[a,b*]

a. Hefei National Laboratory for Physical Sciences at the Microscale, iChem Center, University of Science and Technology of China, Hefei 230026, China
b. CAS Center for Excellence in Quantum Information and Quantum Physics, University of Science and Technology of China, Hefei 230026, China

(Dated: Received on December 1, 2018; Accepted on January 3, 2019)

Saturation spectroscopy is frequently used to obtain sub-Doppler measurement of atomic and molecular transitions. Optical resonant cavities can be used to enhance the effective absorption path length, and the laser power inside the cavity as well to saturate very weak ro-vibrational transitions of molecules. Three different cavity-enhanced methods, cavity enhanced absorption spectroscopy, cavity ring-down spectroscopy, and noise-immune cavity enhanced optical heterodyne molecular spectroscopy (NICE-OHMS), were compared by measuring the Lamb dip of a C_2H_2 line at 1.4 μm using a cavity with a finesse of 120000. The center of the line was determined by different cavity-enhanced methods, each giving a sub-kHz ($\delta\nu/\nu\approx10^{-12}$) statistical uncertainty. The sensitivity and precision of different methods were analyzed and compared. As demonstrated in this study, the NICE-OHMS method is the most sensitive one, but more investigation on the systematic uncertainty is necessary before its application in metrology studies toward a sub-kHz accuracy.

Key words: Precision spectroscopy, Metrology, Cavity enhanced

I. INTRODUCTION

Precision spectroscopy of molecules in the infrared is interested in various studies and applications. They can be used to test fundamental physics [1, 2], to determine fundamental physical constants [3], to investigate intra-molecular dynamics [4], as frequency standards [5, 6], and laboratory spectroscopy data for atmospheric and astronomy observations [7–10]. The accuracy of the transition frequencies derived from molecular spectroscopy measurements is mainly limited by the line width raised from various broadening mechanisms. Saturation absorption (Lamb dip) spectroscopy is one of the most frequently used methods to eliminate the Doppler broadening in a conventional sample cell. However, precise saturation spectroscopy of molecules has been limited to a few molecules (see Ref.[11]). There are two main difficulties in such measurements. The first one is that the transitions are usually very weak, particularly for those overtone transitions in the near-infrared, which have a typical Einstein coefficient of 10^{-4}–10^{-1} s^{-1}. The second one is that the saturation power is often too high to be reached by conventional tunable lasers. As a typical transient-time broadening of 10^2 kHz is the main contribution to the Doppler-free line width of molecules in a gas cell at room temperature, usually a saturation power at the level of kilo-Watts per cm^2 is needed, but conventional diode lasers have only outputs of milli-Watts.

A high-finesse cavity can be used to overcome both difficulties: both the effective absorption path length and the intra-cavity laser power can be enhanced with a factor of 10^3–10^6 by using commercially available high-reflective mirrors. There have been mainly three types of cavity-enhanced methods used for saturation spectroscopy measurements of infrared molecular transitions: cavity enhanced absorption spectroscopy (CEAS), cavity ring-down spectroscopy (CRDS) [12], and noise-immune cavity enhanced optical heterodyne molecular spectroscopy (NICE-OHMS). CEAS has been used to detect Lamb dips of CO_2 around 1.6 μm with a sensitivity of 7.8×10^{-12} cm^{-1} [13]. Since CEAS is based on the measurement of the light power transmitted from the cavity, it often suffers from the power noise of the laser source. CRDS detects the decay rate of the laser power in the cavity, which is naturally immune to the power noise, and eventually improves in the sensitivity. A sensitivity (noise equivalent absorption per unit length, NEAL) of 10^{-13} cm^{-1} has been demonstrated [14] by CRDS. Lamb-dip spectroscopy using

†Dedicated to Professor Kopin Liu on the occasion of his 70th birthday.

*Author to whom correspondence should be addressed. E-mail: smhu@ustc.edu.cn

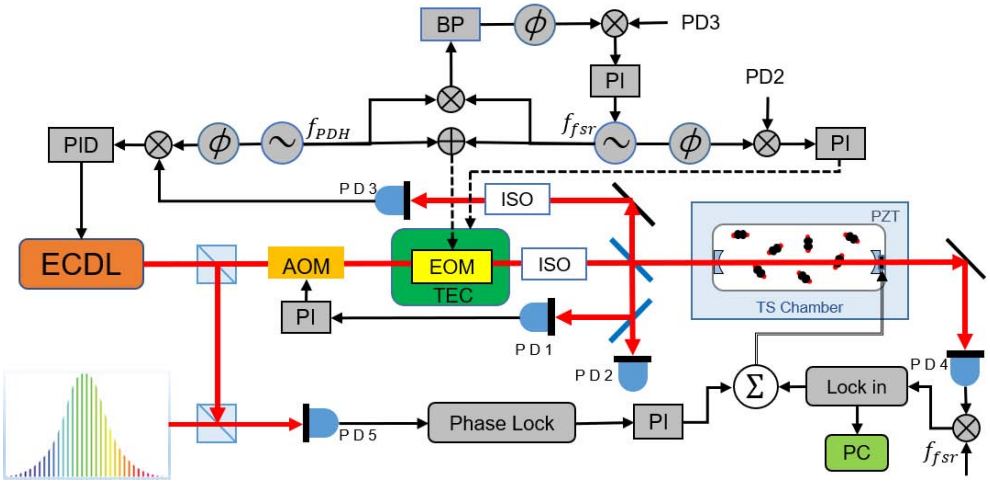

FIG. 1 Configuration of the experimental setup. AOM: acousto-optical modulator, BP: bandpass filter, EOM: electro-optical modulator, ISO: optical isolator, PC: personal computor, PD: photodiode detector, PI: proportion integration amplifier, PZT: piezoelectric actuator, TEC: temperature-control.

CRDS has been recently demonstrated in several groups [11, 15, 16]. NICE-OHMS integrates a frequency modulation of typically 10^2 MHz, being exactly equal to the cavity free spectral range, which reduces not only the laser power noise, $1/f$ noise, but also the laser frequency noise. The technique was first demonstrated as a frequency reference at 1064 nm by Ye *et al.* [17], giving an astonishing sensitivity of 10^{-14} cm^{-1} [18]. This extremely sensitive technique has been applied to lock lasers with molecular transitions [17, 19, 20] without giving the absolute frequencies.

All these three methods have been applied to determine line positions of molecules with kHz or even sub-kHz accuracy. However, recent studies also reveal disagreements between measurements using different methods. For example, NICE-OHMS has been used to detect Lamb dips of a few very weak overtone transitions of HD at 1.39 μm [21], but the position of the R(1) line disagrees with that obtained from CRDS [3]. The reason is yet unknown, indicating that a consistency check between different methods is necessary. Here we present a direct comparison of all these three methods using the same optical cavity to measure an acetylene line at 1.4 μm. Detection sensitivity and accuracy of the line position determined from the spectra obtained by three methods were investigated. Further improvement is expected in the cavity enhanced saturation spectroscopy of molecules, in which a fractional accuracy of 10^{-13} would be very useful in both fundamental science and also applications.

II. EXPERIMENTAL SETUP

A diagram of the experimental setup is presented in FIG. 1. The optical cavity comprises a pair of curved high-reflective (HR) mirrors (Layetec, R=99.997%), with one of the mirrors mounted on a piezoelectric actuator (Core Tomorrow HPst150/20-15/12). The distance between two mirrors is 75 cm, leading to a free spectral range (FSR) of 199 MHz. The finesse of the cavity is determined to be 120000 and the cavity mode width is 1.6 kHz. The optical cavity body is made of aluminum and enclosed in a stainless-steel vacuum chamber, which can be pumped to 10^{-5} Pa by a turbo pump. The aluminum cavity is heated to about 298 K by a heating wire controlled by a feedback servo to stabilize the temperature of the cavity. The outer vacuum chamber is also used as a heat reservoir. The temperature of the aluminum cavity is measured by two thermo-sensors and the fluctuation is found to be 10 mK for hours.

The probe laser is an external-cavity diode laser (Toptica DL100 Pro) with an output power of 50 mW, operating at 1380 nm. The laser is locked with a mode of the optical cavity using the Pound-Drever-Hall (PDH) method. Frequency calibration of the probe laser is implemented by detecting the beat signal between the laser and an optical frequency comb. The comb is synthesized by an Er-fiber Oscillator operated at 1.56 μm. Its repetition frequency ($f_{\rm R}$=198 MHz) and the carrier offset frequency (f_0=250 MHz) are both referenced to a GPS-disciplined rubidium clock (GPS Reference-2000). A phase-lock circuit is used to lock the beat signal to a preset frequency ($f_{\rm B}$) by tuning the optical cavity length through the PZT attached on the HR mirror. In this way, the cavity length and eventually the probe laser frequency are locked with the comb. Frequency scan of the probe laser is realized by tuning the frequency $f_{\rm B}$.

The main beam from the probe laser is first frequency-shifted by an acoustic optics modulator (AOM), phase modulated by an electro-optic modulator (EOM) at a frequency ($f_{\rm PDH}$) of about 20 MHz, and then sent to the high-finesse cavity. The EOM is

DOI:10.1063/1674-0068/cjcp1812272

temperature-stabilized by a TEC unit. Two detectors (PD1 and PD2) are used to monitor the laser power and the parasitic residual modulation effects, respectively. The back reflected light from the cavity is detected by a photo-receiver (PD3), demodulated at 20 MHz, and used to lock the laser frequency to the cavity mode via the PDH scheme. The beam transmitted from the cavity is collected by another detector (PD4).

CEAS signal was directly detected by the photodiode (PD4 in FIG. 1). Wavelength-modulated (WM) CEAS signal was obtained from a lock-in amplifier (SRS 830) when we dither the cavity length through the PZT attached to the HR mirror, which eventually modulates the laser wavelength. Either $1f$ or $2f$ demodulated WM-CEAS signal can be obtained. NICE-OHMS measurements were realized by adding an additional frequency modulation on the EOM with a frequency f_{FSR}. The signal of the beam reflected from the cavity (PD3) is divided into two parts, one is to lock the laser frequency to the cavity via the PDH scheme, and the other one is to lock f_{FSR} to the cavity free spectral range frequency using the DeVoe-Brewer (DVB) scheme [22]. The NICE-OHMS signal was obtained by demodulating the cavity transmittance signal (PD4) at the frequency f_{FSR} by a double balanced mixer (DBM). The output from the DBM is amplified to retrieve the DC dispersive NICE-OHMS signal. Similar to WM-CEAS, wavelength modulated NICE-OHMS signal can also be obtained when the dither signal is applied on the PZT attached on the HR mirror. The scheme for CRDS measurement is similar to that presented in our previous study [11]. It was realized by splitting a beam from the probe laser (not shown in FIG. 1, which is frequency-shifted and sent to the cavity colinearly with the "locking" beam and detected separately.

As we can see, from the experimental point of view, the CEAS method is the simplest one among all these methods, but laser power stabilization is essential to improve its sensitivity. In CRDS measurement, laser power stabilization is not necessary, but we have to couple an additional laser beam into the cavity to keep locking the laser frequency with the cavity, since the probe beam needs to be cut off to initiate ring down event. In NICE-OHMS measurement, only one beam is needed to couple into the cavity, but much more sophisticated locking servos are needed. As we will show below, the accuracy of the NICE-OHMS measurements is also very sensitive to the conditions and quality of these locking servos.

The Lamb dip of the R(4) line in the $\nu_1+\nu_2+(2\nu_4+\nu_5)^1$ band of C_2H_2 was used as an example to test all three methods. The line is located at 7239.7908 cm^{-1}, with an intensity of 4.43×10^{-24} cm/molecule, and an Einstein coefficient of 0.00755 s^{-1}, as given in the HITRAN database [7]. The saturation power is estimated to be about 53 $\mathrm{kW/cm}^2$. The input laser power we used in the measurements was about 14 mW and the light intensity emitted from the cavity was measured to be 0.84 mW. The enhanced factor of the cavity was calculated to be 170000 according to the equations given in Ref.[23]. Therefore, the maximum laser power inside the cavity was estimated to be 140 W. It leads to a saturation parameter of about 0.7 taking into account a laser beam waist radius of 0.46 mm.

III. RESULTS AND DISCUSSION

FIG. 2 shows the C_2H_2 spectra measured by CRDS, CEAS, WM-CEAS ($1f$), and WM-NICE-OHMS ($1f$). Each scan took about 100 s. Different profiles (see below) were used to fit the spectra and the respective fitting residuals are shown in the same figure.

Both CEAS and CRDS directly give absorption spectra which can be modeled by the conventional Lorentzian function

$$S_{\mathrm{L}}(\nu) = \frac{A}{\pi}\cdot\frac{\Gamma}{(\Delta\nu)^2+\Gamma^2} \tag{1}$$

where A is the amplitude, Γ is the half width at half maximum.

Wavelength-modulated CEAS ($1f$) from a lock-in amplifier yields the first derivative of the absorption spectrum,

$$S_{\mathrm{L}}^{\mathrm{wm}}(\nu) = \frac{A}{\pi}\cdot\frac{2}{\tau}\left\{\int_0^{\tau}\frac{\Gamma}{[\Delta\nu+\nu_{\mathrm{a}}\cos(2\pi f_{\mathrm{m}}t)]^2+\Gamma^2}\cdot \cos(2\pi f_{\mathrm{m}}t)\mathrm{d}t\right\} \tag{2}$$

While the spectrum recorded by wavelength-modulated NICE-OHMS ($1f$) can be described by the following function [24]

$$S_{\mathrm{DF}}^{\mathrm{wm}} = \frac{A}{\pi}\cdot\frac{2}{\tau}\left\{\int_0^{\tau}\frac{\delta\nu_{\mathrm{L}}[\Delta\nu+\nu_{\mathrm{a}}\cos(2\pi f_{\mathrm{m}}t)]}{\delta\nu_{\mathrm{L}}^2+[\Delta\nu+\nu_{\mathrm{a}}\cos(2\pi f_{\mathrm{m}}t)]^2}\cdot \cos(2\pi f_{\mathrm{m}}t)\mathrm{d}t\right\} \tag{3}$$

where $\Delta\nu=\nu-\nu_0$ is the detuning from the line center, ν_{a} is the modulation amplitude, $\delta\nu_{\mathrm{L}}$ is the homogeneous linewidth (HWHM), f_{m} is the modulation frequency, and τ is the integral time.

Eq.(1)−Eq.(3) were used to fit the spectra recorded by CRDS and CEAS, CEAS-$1f$, and NICE-OHMS-$1f$, respectively. Parameters including center frequency, width and amplitude of the Lamb dip, together with the modulation amplitude, were derived from the fit.

A. Sensitivity

For better illustration, all the spectra shown in FIG. 2 were normalized using the peak amplitudes. The depth of the Lamb dip observed in CRDS can be directly derived from the ring-down time, which was detected to

DOI:10.1063/1674-0068/cjcp1812272

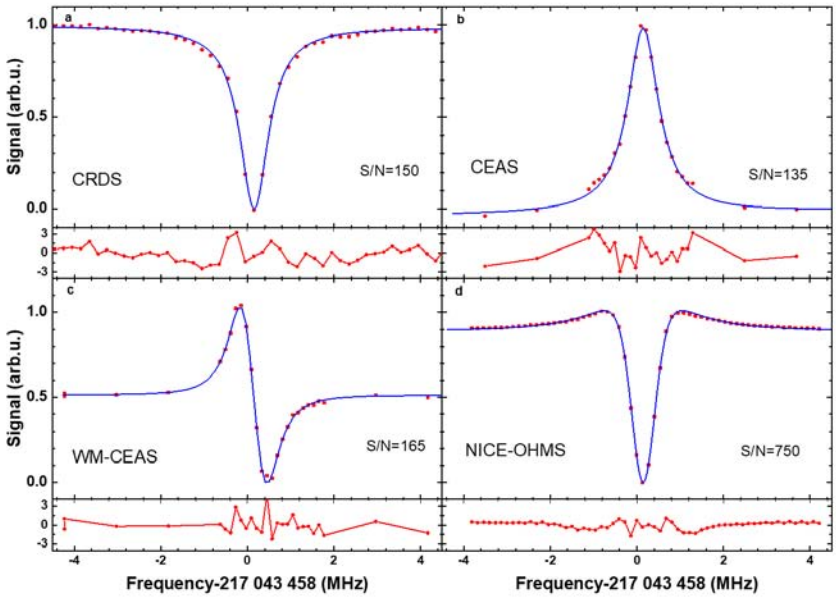

FIG. 2 Saturation spectrum of the R(4) line of C_2H_2 near 7239.79 cm^{-1} recorded by (a) CRDS, (b) CEAS, (c) wavelength-modulated CEAS ($1f$), and (d) wavelength-modulated NICE-OHMS ($1f$). The sample pressure was 1.3 Pa. Fitting residuals were multiplied by a factor of 100.

TABLE I Comparison of the sensitivity and precision of different cavity-enhanced methods by measuring the saturation spectrum of an acetylene line near 1.39 μm.

	Sensitivity/($cm^{-1}Hz^{-1/2}$)	Line position/kHz	Uncertainty/kHz	
			Statistical	Systematic
CRDS	3.5×10^{-11}	217, 043, 458, 146.0	0.8	8.6
CEAS	6.0×10^{-11}	217, 043, 458, 145.5	0.4	5.1
CEAS-$1f$	2.0×10^{-11}	217, 043, 458, 145.0	0.2	2.3
NICE-OHMS-$1f$	5.1×10^{-12}	217, 043, 458, 143.7	0.03	5.0

be 1×10^{-8} cm^{-1}. Consequently, the sensitivity of each method can be readily derived according to the noise level in each spectrum. Table I gives the sensitivities for different methods applied in the measurements.

Noise in CEAS signal mainly comes from the fluctuation in the injected laser power. The power stabilization servo (signal from PD1 shown in FIG. 1) considerably reduces the fast fluctuation in the laser power. However, slow drift, from various sources, such as the reference level used in the servo, remains and contributes a slow drift in the spectrum during the spectral scan. Because CRDS derives the absorption coefficient from the decay rate of the emitted light, in principle, it is less sensitive to the laser power in detecting linear absorption. However, the Lamb dip measurement of CRDS still suffers from the laser power fluctuation [11] because the saturation effect itself depends on the total laser power built-up in the cavity. The laser power, and consequently the saturation absorption signal, both change during recording the ring-down signal in CRDS measurements.

The wavelength modulation effectively reduced the baseline drift in CEAS and resulted in an improved signal-to-noise ratio (SNR). Note that the WM technique cannot be used in the CRDS measurement, finally we obtained similar SNR in both CRDS and WM-CEAS measurements. In general, NICE-OHMS is more sensitive than both CRDS and CEAS, since both the $1/f$ noise and the phase noise of the laser can be effectively eliminated in NICE-OHMS. FIG. 2(d) shows the wavelength modulated NICE-OHMS spectrum of the R(4) line of acetylene. SNR in the spectrum was about 750, 5 times of that obtained in CRDS. Consequently, the statistical uncertainty obtained from NICE-OHMS is considerably smaller than that from other methods.

B. Precision

In order to determine the line position of the C_2H_2 line, 720 CEAS scans were recorded in about 10 h, and the spectra were fitted using the Lorentzian function with a baseline (linear function). The observed linewidth was about 370 kHz (half width at half maximum), as a result of the transit-time width (180 kHz), plus power broadening and pressure broadening. The

DOI:10.1063/1674-0068/cjcp1812272

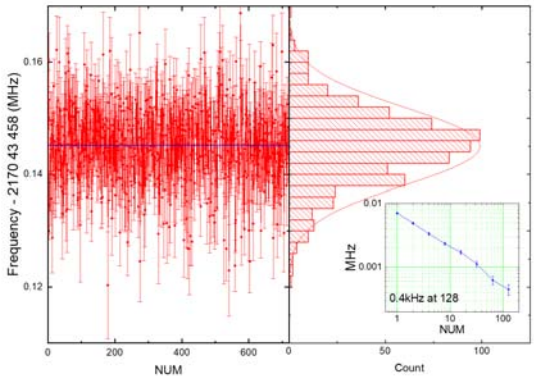

FIG. 3 Statistics of the R(4) line position determined by cavity-enhanced absorption spectroscopy. Inset: Allan deviation of the R(4) line position.

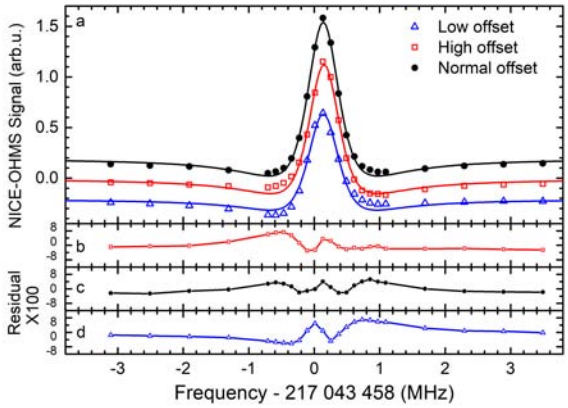

FIG. 4 Spectra of the R(4) line of C_2H_2 recorded at different offsets applied in the NICE-OHMS measurements.

line centers derived from the fit are illustrated in FIG. 3. The averaged line center is 217, 043, 458, 145.5 kHz with a statistical uncertainty of 0.4 kHz. The Allan deviation of the line centers versus the number of averaging is shown in FIG. 3, indicating that the statistical uncertainty is approximately 6 kHz/$\sqrt{N}$ where N is the averaging number.

Spectra recorded with other methods were also used to derive the line center, and the results are given in Table I. In total, 20, 720, 70, 100 scans were used in CRDS, CEAS, WM-CEAS, and NICE-OHMS measurements, respectively, which yields statistical uncertainties of 0.8, 0.4, 0.2, and 0.03 kHz. The positions obtained from different methods have discrepancies below 3 kHz, which are mainly due to the systematic uncertainties in different measurements and they are discussed below.

The uncertainty in the frequency calibration was 0.4 kHz from the rubidium clock which has a monthly fluctuation of about 2×10^{-12}. The radio frequency source (Rigol DG4202) and frequency counter (Agilent 53181A) were both referenced to the rubidium clock, and the uncertainty in $f_{\rm B}$ was well below 1 kHz. However, due to the increased noise level in the frequency lock during the CRDS measurement, the uncertainty in the $f_{\rm B}$ signal was as high as 5 kHz.

The main systematic uncertainty in the Lamb dip measurements is that from the asymmetry in the line profile. The line profile was considered to be symmetric in the spectral fitting, however, there is often asymmetry observed in the spectra due to various reasons. As the fitting residuals shown in FIG. 2, we cannot exclude possible asymmetry around the line center. Such asymmetry would result in a shift in the position derived from the fit. We can conservatively estimate the asymmetry-induced shifts according to the fitting residuals observed in different measurements,

$$\delta = \Delta_{\rm H} \cdot \left| \frac{d_{\rm max}}{A} \right| \tag{4}$$

where $\Delta_{\rm H}$ is the half width at the half maximum of the line, $d_{\rm max}$ is the maximum of the fitting residual, and A is the amplitude of the signal. Therefore, we estimate uncertainties due to the asymmetry in the profile are 7 kHz, 5 kHz, 2 kHz and 3 kHz for CRDS, CEAS, WM-CEAS and NICE-OHMS results, respectively.

Although NICE-OHMS is considered more sensitive than CEAS and CRDS, which gives a much smaller statistical uncertainty in the line center, we found that the reproducibility of the line center value determined by NICE-OHMS was considerably worse. Because more complicated phase modulation is applied in NICE-OHMS, it makes the line profile much more sensitive to some experimental conditions. FIG. 4 illustrates the recorded NICE-OHMS spectra when different reference offsets were applied in the PDH locking. Note that the choice of the reference offset is somehow ambiguous since usually it only changes slightly the characteristic response of the locking servo. The resulted change in the laser frequency is well below 0.1 kHz, which should not affect the spectral signal. However, as shown in the fitting residuals given in the figure, there are obvious change in the recorded line profile. Asymmetry in the line profile considerably changes the line center derived from the fit of the profile. Therefore, an additional systematic uncertainty must be considered in NICE-OHMS. Moreover, since the NICE-OHMS technique is based on the phase modulation of the sidebands at the two adjacent cavity modes at both sides of the carrier, any unbalance between these two sidebands, such as the influence from a nearby absorption line, would result in asymmetry in the line profile. Our analysis indicates that more investigation is needed on the line position retrieved from the NICE-OHMS measurement. As a result, here we estimate a systematic uncertainty of 5.0 kHz in the line position derived from the NICE-OHMS measurement.

Taking into account the uncertainties discussed above, we assess the systematic uncertainties for the R(4) line center for different methods, and they are

DOI:10.1063/1674-0068/cjcp1812272

given in Table I. The line centers obtained from different methods agree with each other within the uncertainties. If we take a weighted average of the positions given by different methods, we determine the position of the R(4) line to be 217, 043, 458, 144.9±2.0 kHz (7239.79047348(7) cm^{-1}). The position agrees with the value 7239.79077(198) cm^{-1} previously reported by Vander Auwera *et al.* [25] using Doppler-limited spectroscopy, while the accuracy has been improved by four orders of magnitude.

IV. CONCLUSION

In summary, we have performed a comparison of different cavity-enhanced saturation spectroscopy methods, CRDS, CEAS and NICE-OHMS, by using one setup and measuring an overtone transition of acetylene at 1380 nm. In general, the NICE-OHMS spectrum has better SNR compared to other methods. All three methods can give a statistical uncertainty at the sub-kHz level. However, one must consider the asymmetry in the NICE-OHMS spectral profile which is correlated with the experimental parameters applied in the measurements. CEAS and CRDS are relatively simple without using too many sophisticated modulations. CRDS is more sensitive than conventional CEAS, but more efforts are needed if one wants to derive quantitative line profile from Lamb-dip measurements using CRDS. By adopting dedicated control servos to reduce both the power and phase noise of the probe laser, we established wavelength-modulated CEAS measurements which have almost the same SNR as CRDS. By using all these cavity-enhanced methods, we measured the Lamb dip spectrum of the R(4) line in the $\nu_1+\nu_2+(2\nu_4+\nu_5)^1$ band of C_2H_2. After an analysis of the uncertainties from various sources, we determine the line center to be 217 043 458 144.9(±2.0) kHz, as a weighted average of the results obtained from different methods. Since a huge amount of molecular transitions in the infrared can be measured in this way, it can considerably improve the precision of the spectral data of molecules.

V. ACKNOWLEDGEMENTS

This work was supported by the National Natural Science Foundation of China (No.21688102, No.91436209, and No.21427804), and the Chinese Academy of Science (No.XDB21020100).

[1] A. Shelkovnikov, R. J. Butcher, C. Chardonnet, and A. Amy-Klein, Phys. Rev. Lett. **100**, 150801 (2008).
[2] M. Quack, J. Stohner, and M. Willeke, Annu. Rev. Phys. Chem. **59**, 741 (2008).
[3] L. G. Tao, A. W. Liu, K. Pachucki, J. Komasa, Y. R. Sun, J. Wang, and S. M. Hu, Phys. Rev. Lett. **120**, 153001 (2018).
[4] A. W. Liu, X. F. Li, J. Wang, Y. Lu, C. F. Cheng, Y. R. Sun, and S. M. Hu, J. Chem. Phys. **138**, 014312 (2013).
[5] S. M. Foreman, A. Marian, J. Ye, E. A. Petrukhin, M. A. Gubin, O. D. Mucke, F. N. C. Wong, E. P. Ippen, and F. X. Kartner, Opt. Lett. **30**, 570 (2005).
[6] S. Okubo, H. Nakayama, K. Iwakuni, H. Inaba, and H. Sasada, Opt. Expr. **19**, 23878 (2011).
[7] I. E. Gordon, L. S. Rothman, C. Hill, R. V. Kochanov, Y. Tan, P. F. Bernath, M. Birk, V. Boudon, A. Campargue, K. V. Chance, B. J. Drouin, J. M. Flaud, R. R. Gamache, J. T. Hodges, D. Jacquemart, V. I. Perevalov, A. Perrin, K. P. Shine, M. A. H. Smith, J. Tennyson, G. C. Toon, H. Tran, V. G. Tyuterev, A. Barbe, A. G. Császár, V. M. Devi, T. Furtenbacher, J. J. Harrison, J. M. Hartmann, A. Jolly, T. J. Johnson, T. Karman, I. Kleiner, A. A. Kyuberis, J. Loos, O. M. Lyulin, S. T. Massie, S. N. Mikhailenko, N. Moazzen-Ahmadi, H. S. P. Müller,O. V. Naumenko, A. V. Nikitin, O. L. Polyansky, M. Rey, M. Rotger, S. W. Sharpe, K. Sung, E. Starikova, S. A. Tashkun, J. V. Auwera, G. Wagner, J. Wilzewski, P. Wcis lo, S. Yu, and E. J. Zak, J. Quant. Spectrosc. Radiat. Transfer **203**, 3 (2017).
[8] S. M. Hu, H. Pan, C. F. Cheng, Y. R. Sun, X. F. Li, J. Wang, A. Campargue, and A. W. Liu, Astrophys. J. **749**, 76 (2012).
[9] Y. Lu, A. W. Liu, X. F. Li, J. Wang, C. F. Cheng, Y. R. Sun, R. Lambo, and S. M. Hu, Astrophys. J. **775**, (2013).
[10] G. Li, E. G. Iouli, S. R. Laurence, Y. Tan, S. M. Hu, K. Samir, C. Alain, and S. M. Emile, Astrophys. J. Supp. Ser. **216**, 15 (2015).
[11] J. Wang, Y. R. Sun, L. G. Tao, A. W. Liu, and S. M. Hu, J. Chem. Phys. **147**, 091103 (2017).
[12] A. Okeefe and D. A. G. Deacon, Rev. Sci. Instrum. **59**, 2544 (1988).
[13] D. Gatti, R. Gotti, A. Gambetta, M. Belmonte, G. Galzerano, P. Laporta, and M. Marangoni, Sci. Rep. **6**, 27183 (2016).
[14] S. Kassi and A. Campargue, J. Chem. Phys. **137**, 234201 (2012).
[15] G. Giusfredi, S. Bartalini, S. Borri, P. Cancio, I. Galli, D. Mazzotti, and P. De Natale, Phys. Rev. Lett. **104**, 110801 (2010).
[16] S. Kassi, T. Stoltmann, M. Casado, M. Daeron, and A. Campargue, J. Chem. Phys. **148**, 054201 (2018).
[17] J. Ye, L. S. Ma, and J. L. Hall, Opt. Lett. **21**, 1000 (1996).
[18] J. Ye, L. S. Ma, and J. L. Hall, J. Opt. Soc. Am. B **15**, 6 (1998).
[19] T. L. Chen and Y. W. Liu, Opt. Lett. **42**, 2447 (2017).
[20] S. Saraf, P. Berceau, A. Stochino, R. Byer, and J. Lipa, Opt. Lett. **41**, 2189 (2016).
[21] F. M. J. Cozijn, P. Dupré, E. J. Salumbides, K. S. E. Eikema, and W. Ubachs, Phys. Rev. Lett. **120**, 153002 (2018).
[22] R. G. DeVoe and R. G. Brewer, Phys. Rev. A **30**, 2827 (1984).
[23] J. Wang, Y. R. Sun, L. G. Tao, A. W. Liu, T. P. Hua, F. Meng, and S. M. Hu, Rev. Sci. Instrum. **88**, 043108 (2017).
[24] A. Foltynowicz, W. Ma, and O. Axner, Opt. Express **16**, 14689 (2008).
[25] J. Vander Auwera, R. El Hachtouki, and L. R. Brown, Mol. Phys. **100**, 3563 (2002).

DOI:10.1063/1674-0068/cjcp1812272